

1

<sup>2</sup>A SEARCH FOR LONG-LIVED, CHARGED, SUPERSYMMETRIC PARTICLES  
<sup>3</sup>USING IONIZATION WITH THE ATLAS DETECTOR

4

BRADLEY AXEN

5

September 2016 – Version 0.17

6



<sup>8</sup> Bradley Axen: *A Search for Long-Lived, Charged, Supersymmetric Particles using Ion-  
<sup>9</sup> ization with the ATLAS Detector*, Subtitle, © September 2016

10

Usually a quotation.

11

Dedicated to.



<sub>12</sub> ABSTRACT

---

<sub>13</sub> How to write a good abstract:

<sub>14</sub> <https://plg.uwaterloo.ca/~migod/research/beck00PSLA.html>



<sub>15</sub> PUBLICATIONS

---

<sub>16</sub> Some ideas and figures have appeared previously in the following publications:

<sub>17</sub>

<sub>18</sub> Put your publications from the thesis here. The packages `multibib` or `bibtopic`  
<sub>19</sub> etc. can be used to handle multiple different bibliographies in your document.



---

<sup>21</sup> ACKNOWLEDGEMENTS

<sup>22</sup> Put your acknowledgements here.

<sup>23</sup>

<sup>24</sup> And potentially a second round.

<sup>25</sup>



26 CONTENTS

---

27	I	INTRODUCTION	1
28	1	INTRODUCTION	3
29	II	THEORETICAL CONTEXT	5
30	2	STANDARD MODEL	7
31	2.1	Particles . . . . .	7
32	2.2	Interactions . . . . .	8
33	2.3	Limitations . . . . .	8
34	3	SUPERSYMMETRY	9
35	3.1	Motivation . . . . .	9
36	3.2	Structure . . . . .	9
37	3.3	Phenomenology . . . . .	9
38	4	LONG-LIVED PARTICLES	11
39	4.1	Mechanisms . . . . .	11
40	4.1.1	Examples in Supersymmetry . . . . .	11
41	4.2	Phenomenology . . . . .	11
42	4.2.1	Disimilarities to Prompt Decays . . . . .	11
43	4.2.2	Characteristic Signatures . . . . .	11
44	III	EXPERIMENTAL STRUCTURE AND RECONSTRUCTION	13
45	5	THE LARGE HADRON COLLIDER	15
46	5.1	Injection Chain . . . . .	15
47	5.2	Design and Parameters . . . . .	15
48	5.3	Luminosity . . . . .	15
49	6	THE ATLAS DETECTOR	17
50	6.1	Coordinate System . . . . .	17
51	6.2	Magnetic Field . . . . .	17
52	6.3	Inner Detector . . . . .	17
53	6.3.1	Pixel Detector . . . . .	17
54	6.3.2	Semiconductor Tracker . . . . .	17
55	6.3.3	Transition Radiation Tracker . . . . .	17
56	6.4	Calorimetry . . . . .	17
57	6.4.1	Electromagnetic Calorimeters . . . . .	17
58	6.4.2	Hadronic Calorimeters . . . . .	17
59	6.4.3	Forward Calorimeters . . . . .	17
60	6.5	Muon Spectrometer . . . . .	17
61	6.6	Trigger . . . . .	17
62	6.6.1	Trigger Scheme . . . . .	17
63	6.6.2	Missing Transverse Energy Triggers . . . . .	17
64	7	EVENT RECONSTRUCTION	19
65	7.1	Tracks and Vertices . . . . .	19

66	7.1.1	Track Reconstruction . . . . .	19
67	7.1.2	Vertex Reconstruction . . . . .	19
68	7.2	Jets . . . . .	19
69	7.2.1	Topological Clustering . . . . .	19
70	7.2.2	Jet Energy Scale . . . . .	19
71	7.2.3	Jet Energy Scale Uncertainties . . . . .	19
72	7.2.4	Jet Energy Resolution . . . . .	19
73	7.3	Electrons . . . . .	19
74	7.3.1	Electron Identification . . . . .	19
75	7.4	Muons . . . . .	19
76	7.4.1	Muon Identification . . . . .	19
77	7.5	Missing Transverse Energy . . . . .	19
78	IV	CALORIMETER RESPONSE	21
79	8	RESPONSE MEAUREMENT WITH SINGLE HADRONS	23
80	8.1	Overview and Motivation . . . . .	23
81	8.2	Dataset and Simulation . . . . .	24
82	8.2.1	Data Samples . . . . .	24
83	8.2.2	Simulated Samples . . . . .	24
84	8.2.3	Event Selection . . . . .	24
85	8.3	Inclusive Hadron Response . . . . .	25
86	8.3.1	E/p Distribution . . . . .	25
87	8.3.2	Zero Fraction . . . . .	27
88	8.3.3	Neutral Background Subtraction . . . . .	27
89	8.3.4	Corrected Response . . . . .	29
90	8.4	Identified Particle Response . . . . .	29
91	9	JET ENERGY RESPONSE AND UNCERTAINTY	31
92	9.1	Jet Energy Response in Simulation . . . . .	31
93	9.2	Jet Energy Uncertainty . . . . .	31
94	V	SEARCH FOR LONG-LIVED PARTICLES	33
95	10	LONG-LIVED PARTICLES IN ATLAS	35
96	10.1	Overview and Characteristics . . . . .	35
97	10.2	Simulation . . . . .	35
98	11	EVENT SELECTION	37
99	11.1	Trigger . . . . .	37
100	11.2	Kinematics and Isolation . . . . .	37
101	11.3	Standard Model Rejection . . . . .	37
102	11.4	Ionization . . . . .	37
103	11.4.1	dE/dx Calibration . . . . .	37
104	11.4.2	Mass Estimation . . . . .	37
105	12	BACKGROUND ESTIMATION	39
106	12.1	Background Sources . . . . .	39
107	12.2	Prediction Method . . . . .	39
108	12.3	Validation and Uncertainty . . . . .	39
109	13	SYSTEMATIC UNCERTAINTIES AND RESULTS	41

110	13.1 Systematic Uncertainties . . . . .	41
111	13.2 Final Yields . . . . .	41
112	14 INTERPRETATION	43
113	14.1 Cross Sectional Limits . . . . .	43
114	14.2 Mass Limits . . . . .	43
115	14.3 Context for Long-Lived Searches . . . . .	43
116	<b>VI CONCLUSIONS</b>	45
117	15 SUMMARY AND OUTLOOK	47
118	15.1 Summary . . . . .	47
119	15.2 Outlook . . . . .	47
120	<b>VII APPENDIX</b>	49
121	A INELASTIC CROSS SECTION	51
122	B APPENDIX TEST	53
123	B.1 Appendix Section Test . . . . .	53
124	B.1.1 Appendix Subection Test . . . . .	53
125	B.2 A Table and Listing . . . . .	53
126	B.3 Some Formulas . . . . .	54
127	<b>BIBLIOGRAPHY</b>	57

128 LIST OF FIGURES

---

129	Figure 1	The particle content of the Standard Model. . . . .	8
130	Figure 2	An illustration (a) of the $E/p$ variable used throughout this paper. The red energy deposits come from the charged particle targeted for measurement, while the blue energy deposits are from nearby neutral particles and must be subtracted. The same diagram (b) for the neutral-background selection, described in Section 8.3.3.	26
131			
132			
133			
134			
135			
136	Figure 3	The $E/p$ distribution and ratio of simulation to data for isolated tracks with (a) $ \eta  < 0.6$ and $1.2 < p/\text{GeV} < 1.8$ and (b) $ \eta  < 0.6$ and $2.2 < p/\text{GeV} < 2.8$ . . . . .	26
137			
138			
139	Figure 4	The fraction of tracks as a function (a, b) of momentum, (c, d) of interaction lengths with $E \leq 0$ for tracks with positive (on the left) and negative (on the right) charge. . . . .	28
140			
141			
142			
143	Figure 5	$\langle E/p \rangle_{\text{BG}}$ as a function of the track momentum and (a) $ \eta  < 0.6$ , (b) $0.6 <  \eta  < 1.1$ , and as a function of the track pseudorapidity and (c) $1.2 < p/\text{GeV} < 1.8$ , (d) $1.8 < p/\text{GeV} < 2.2$ . . . . .	29
144			
145			
146			

<sup>147</sup> LIST OF TABLES

---

<sup>148</sup> Table 1	Autem usu id . . . . .	53
------------------------	------------------------	----

<sub>149</sub> LISTINGS

---

<sub>150</sub>	Listing 1	A floating example ( <code>listings</code> manual) . . . . .	54
----------------	-----------	--	----

152 EG Example



153

## PART I

154

### INTRODUCTION

155

You can put some informational part preamble text here.



# 1

156

157 INTRODUCTION

---



158

## PART II

159

### THEORETICAL CONTEXT

160

You can put some informational part preamble text here.



# 2

161

## 162 STANDARD MODEL

---

163 The Standard Model of particle physics seeks to explain the symmetries and in-  
164 teractions of all currently discovered fundamental particles. It has been tested by  
165 several generations of experiments and has been remarkably successful, no sig-  
166 nificant deviations have been found. The Standard Model provides predictions  
167 in particle physics for interactions up to the Planck scale ( $10^{15}$ - $10^{19}$  GeV).

168 The theory itself is a quantum field theory grown from an underlying  $SU(3) \times$   
169  $SU(2) \times U(1)$  that requires the particle content and quantum numbers consist-  
170 ent with experimental observations (see Section 2.1). Each postulated symme-  
171 try is accompanied by an interaction between particles through gauge invari-  
172 ance. These interactions are referred to as the Strong, Weak, and Electromag-  
173 netic forces, which are discussed in Section 2.2.

174 Although this model has been very predictive, the theory is incomplete; for  
175 example, it is not able to describe gravity or astronomically observed dark matter.  
176 These limitations are discussed in more detail in Section 2.3.

## 177 21 PARTICLES

178 The most familiar matter in the universe is made up of protons, neutrons, and  
179 electrons. Protons and neutrons are composite particles, however, and are made  
180 up in turn by particles called quarks. Quarks carry both electric charge and color  
181 charge, and are bound in color-neutral combinations called baryons. The elec-  
182 tron is an example of a lepton, and carries only electric charge. Another type  
183 of particle, the neutrino, does not form atomic structures in the same way that  
184 quarks and leptons do because it carries no color or electric charge. Collectively,  
185 these types of particles are known as fermions, the group of particles with half-  
186 integer spin.

187 There are three generations of fermions, although familiar matter is formed  
188 predominantly by the first generation. The generations are identical except for  
189 their masses, which increase in each generation by convention. In addition, each  
190 of these particles is accompanied by an antiparticle, with opposite-sign quantum  
191 numbers but the same mass.

192 The fermions comprise what is typically considered matter, but there are  
193 additional particles that are mediators of interactions between those fermions.  
194 These mediators are known as the gauge bosons, gauge in that their existence  
195 is required by gauge invariance (discussed further in Section 2.2) and bosons in  
196 that they have integer spin. The boson which mediates the electromagnetic force  
197 is the photon, the first boson to be discovered; it has no electric charge, no mass,  
198 and a spin of 1. There are three spin-1 mediators of the weak force, the two W  
199 bosons and the Z boson. The W bosons have electric charge of  $\pm 1$  and a mass of  
200  $80.385 \pm 0.015$  GeV, while the Z boson is neutral and has a mass of  $91.1876 \pm$

201 0.0021 GeV. The strong force is mediated by eight particles called gluons, which  
 202 are massless and electrically neutral but do carry color charge.

203 The final particle present in the Standard Model is the Higgs boson, which was  
 204 recently observed for the first time by experiments at CERN in 2012. It is electric-  
 205 ally neutral, has a mass of  $125.7 \pm 0.4$  GeV, and is the only spin-0 particle yet to  
 206 be observed. The Higgs boson is the gauge boson associated with the mechanism  
 207 that gives a mass to the W and Z bosons.

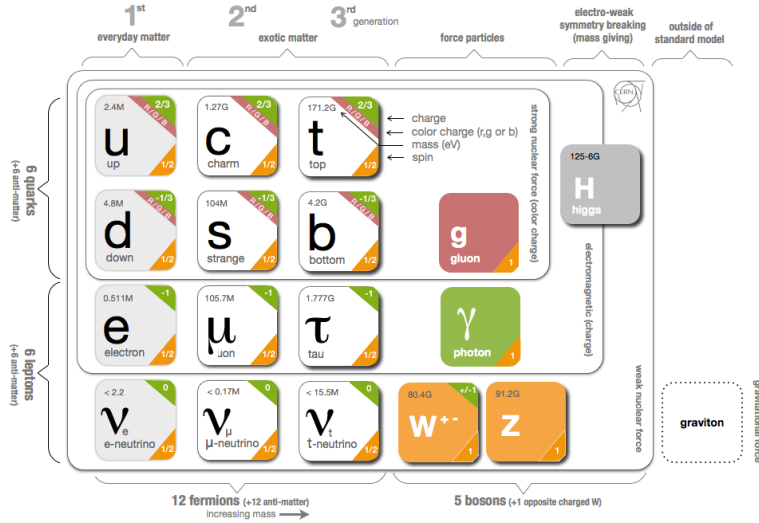


Figure 1: The particle content of the Standard Model.

208 Together these particles form the entire content of the Standard Model, and  
 209 are summarized in Figure 1. These are the particles that constitute the observable  
 210 universe and all the so-far-observed interactions within it.

## 211 2.2 INTERACTIONS

212 The interactions predicted and described by the Standard Model are fundamen-  
 213 tally tied to the particles within it, both in that they describe the way those par-  
 214 ticles can influence each other and also in that the existence of the interactions  
 215 requires the existence of some particles (the gauge bosons).

## 216 2.3 LIMITATIONS

# 3

217

218 SUPERSYMMETRY

---

219 3.1 MOTIVATION

220 3.2 STRUCTURE

221 3.3 PHENOMENOLOGY



# 4

222

223 LONG-LIVED PARTICLES

---

224 4.1 MECHANISMS

225 4.1.1 EXAMPLES IN SUPERSYMMETRY

226 4.2 PHENOMENOLOGY

227 4.2.1 DISIMILARITIES TO PROMPT DECAYS

228 4.2.2 CHARACTERISTIC SIGNATURES



229

### PART III

230

## EXPERIMENTAL STRUCTURE AND RECONSTRUCTION

231

You can put some informational part preamble text here.



# 5

232

233 THE LARGE HADRON COLLIDER

---

234 5.1 INJECTION CHAIN

235 5.2 DESIGN AND PARAMETERS

236 5.3 LUMINOSITY



# 6

237

## 238 THE ATLAS DETECTOR

---

239 6.1 COORDINATE SYSTEM

240 6.2 MAGNETIC FIELD

241 6.3 INNER DETECTOR

242 6.3.1 PIXEL DETECTOR

243 6.3.2 SEMICONDUCTOR TRACKER

244 6.3.3 TRANSITION RADIATION TRACKER

245 6.4 CALORIMETRY

246 6.4.1 ELECTROMAGNETIC CALORIMETERS

247 6.4.2 HADRONIC CALORIMETERS

248 6.4.3 FORWARD CALORIMETERS

249 6.5 MUON SPECTROMETER

250 6.6 TRIGGER

251 6.6.1 TRIGGER SCHEME

252 6.6.2 MISSING TRANSVERSE ENERGY TRIGGERS



# 7

253

## 254 EVENT RECONSTRUCTION

---

255 The ATLAS experiment combines measurements in the subdetectors to form a  
256 cohesive picture of each physics event.

## 257 7.1 TRACKS AND VERTICES

### 258 7.1.1 TRACK RECONSTRUCTION

#### 259 7.1.1.1 NEURAL NETWORK

#### 260 7.1.1.2 PIXEL DE/DX

#### 261 7.1.2 VERTEX RECONSTRUCTION

## 262 7.2 JETS

### 263 7.2.1 TOPOLOGICAL CLUSTERING

### 264 7.2.2 JET ENERGY SCALE

### 265 7.2.3 JET ENERGY SCALE UNCERTAINTIES

### 266 7.2.4 JET ENERGY RESOLUTION

## 267 7.3 ELECTRONS

### 268 7.3.1 ELECTRON IDENTIFICATION

## 269 7.4 MUONS

### 270 7.4.1 MUON IDENTIFICATION

## 271 7.5 MISSING TRANSVERSE ENERGY



272

## PART IV

273

### CALORIMETER RESPONSE

274

You can put some informational part preamble text here.



275

276 RESPONSE MEAUREMENT WITH SINGLE HADRONS

---

## 277 8.1 OVERVIEW AND MOTIVATION

278 As discussed in Section 7.2, colored particles produced in collisions hadronize  
279 into jets of multiple individual hadrons. As jets form a major component of many  
280 physics analyses at ATLAS, it is crucial to carefully calibrate the measurement of  
281 jet energies and to derive an uncertainty on that measurement. These uncertain-  
282 ties have often been the dominant systematic uncertainty in high-energy analy-  
283 ses at the LHC.

284 One approach to understanding jet physics in the ATLAS calorimetry is to  
285 evaluate the calorimeter response to individual hadrons; measurements of indi-  
286 vidual hadrons can be used to build up an understanding of the jets that they form.  
287 The redundancy of the momentum provided by the tracking system and the en-  
288 ergy provided by the calorimeter provides an opportunity to study calorimeter  
289 response using real collisions, as described further in Section 8.3.

290 A number of interesting factors compromise calorimeter response, and extract-  
291 ing these separately provides insight into many aspects of jet modelling. First,  
292 many charged hadrons interact with the material of the detector prior to reach-  
293 ing the calorimeters and thus do not deposit any energy. Comparing this effect in  
294 data and simulation is a powerful tool in validating the interactions of particles  
295 with the material of the detector as well as the model of the detector geometry  
296 in simulation, see Section 8.3.2. The particles which do reach the calorimeter de-  
297 posit their energy into individual cells, which are then clustered to measure full  
298 energy deposits. Comparing the response in data to simulated hadrons provides  
299 a direct evaluation of several aspects of simulation: noise in the calorimeters, the  
300 showering of hadronic particles, and the energy deposited by particles in matter,  
301 among others (Section 8.3.4). Additionally, comparing the effect of clustering in  
302 data and simulation can indirectly test the simulation’s modelling of the shape  
303 of hadronic showers, see Section 8.3.4.1. These measurements are extended to  
304 explore several additional effects, such as the dependence on charge or the indi-  
305 vidual calorimeter layer in Section 8.3.4.2.

306 The above studies all use an inclusive selection of charged particles, which are  
307 compromised predominantly of pions, kaons, and (anti)protons. It is also inter-  
308 esting to measure the particle types separately to evaluate the simulated inter-  
309 actions of each particle, particularly at low energies where differences between  
310 species are very relevant. Pions and (anti)protons can be identified through de-  
311 cays of long-lived particles, in particular  $\Lambda$ ,  $\bar{\Lambda}$ , and  $K_S^0$ , and then used to measure  
312 response as described above. This is discussed in detail in Section 8.4.

313 Together, these measurements in data provide a thorough understanding of  
314 the way hadrons interact with the ATLAS detector and can be used to build up a  
315 description of jets, as seen in Chapter 9. The results in this chapter use data col-

316 lected at 7 and 8 TeV collected in 2010 and 2012, respectively. Both are included  
 317 as the calorimeter was repaired and recalibrated between those two data-taking  
 318 periods. Both sets of data are compared to an updated simulation that includes  
 319 new physics models provided by `Geant4` [7] and improvements in the detector  
 320 description [2, 5]. These results can be compared to a similar measurement per-  
 321 formed in 2009 and 2010 [4], which used the previous version of the simulation  
 322 framework [1].

## 323 8.2 DATASET AND SIMULATION

### 324 8.2.1 DATA SAMPLES

325 The two datasets used in this chapter are taken from dedicated low-pileup runs  
 326 where the fraction of events with multiple interactions was negligible, to facil-  
 327 itate measurement of isolated hadrons. The 2012 dataset at  $\sqrt{s} = 8$  TeV contains 8  
 328 million events and corresponds to an integrated luminosity of  $0.1 \text{ nb}^{-1}$ . The 2010  
 329 dataset at  $\sqrt{s} = 7$  TeV contains 3 million events and corresponds to an integrated  
 330 luminosity of  $3.2 \text{ nb}^{-1}$ . This last dataset was also used in the 2010 results [4], but  
 331 have since been reanalyzed with an updated detector description of the material  
 332 and alignment.

### 333 8.2.2 SIMULATED SAMPLES

334 The two datasets above are compared to simulated single-, double-, and non-  
 335 diffractive events generated with `Pythia8` [24] using the A2 configuration of  
 336 hadronization [3] and the MSTW 2008 parton-distribution function set [20, 23].  
 337 The conditions and energies for each run are matched in the two simulations.

338 To evaluate the interaction of hadrons with detector material, the simulation  
 339 uses two different collections of hadronic physics models, called physics lists, in  
 340 `Geant4` 9.4 [22]. The first, `QGSP_BERT`, combines the Bertini intra-nuclear  
 341 cascade [12, 18, 19] below 9.9 GeV, a parametrized proton inelastic model from  
 342 9.5 to 25 GeV [15], and a quark-gluon string model above 12 GeV [8, 9, 13, 14,  
 343 16]. The second, `FTFP_BERT`, combines the Bertini intra-nuclear cascade [12, 18,  
 344 19] below 5 GeV and the Fritiof model [10, 11, 17, 21] above 4 GeV. In either list,  
 345 where multiple models overlap, the transition between the two models is ensured  
 346 to be smooth.

### 347 8.2.3 EVENT SELECTION

348 The event selection for this study is minimal, as the only requirement is selecting  
 349 good-quality events with an isolated track. Such events are triggered by requir-  
 350 ing at least two hits in the minimum-bias trigger scintillators. After trigger, each  
 351 event is required to have exactly one reconstructed vertex, and that vertex is re-  
 352 quired to have four or more associated tracks.

353     The particles which enter into the response measurements are first identified  
 354     as tracks in the inner detector. To ensure a reliable momentum measurement,  
 355     these tracks are required to have at least one hit in the pixel detector, six hits in  
 356     the SCT, and small longitudinal and transverse impact parameters with respect  
 357     to the primary vertex [4]. For the majority of the measurements in this chapter,  
 358     the track is additionally required to have 20 hits in the TRT, which significantly  
 359     reduces the contribution from tracks which undergo nuclear interaction. This  
 360     requirement and its effect is discussed in more detail in Section ?? . In addition,  
 361     tracks are rejected if there is another track which extrapolates to the calorimeter  
 362     within a cone of  $\Delta R = \sqrt{(\Delta\phi)^2 + (\Delta\eta)^2} < 0.4$ . This requirement guarantees  
 363     that the contamination of energy from nearby charged particles is negligible [4].

### 364     8.3 INCLUSIVE HADRON RESPONSE

365     The calorimeter response is more precisely defined as the ratio of the measured  
 366     calorimeter energy to the true energy carried by the particle, although this true  
 367     energy is unknown. For charged particles, however, the inner detector provides  
 368     a very precise measurement of momentum (with uncertainty less than 1%) that  
 369     can be used as a proxy for true energy. The ratio of the energy deposited by the  
 370     charged particle in the calorimeter,  $E$ , to its momentum measured in the inner  
 371     detector  $p$ , forms the calorimeter response measure called  $E/p$ . Though the dis-  
 372     tribution of  $E/p$  is interesting, two aggregated quantities are more directly use-  
 373     ful:  $\langle E/p \rangle$ , the average of  $E/p$  within a given subset of particles, and the zero  
 374     fraction, the fraction of particles with no associated clusters in the calorimeter.

375     The calorimeter energy assigned to a track particle is defined using either cells  
 376     or clusters. When clusters are used, they are formed using a 4–2–0 algorithm [6]  
 377     that begins with seeds requiring at least 4 times the calorimeter average noise.  
 378     The neighboring cells with at least twice that noise threshold are then added to  
 379     the cluster, and all bounding cells are then added with no requirement. This algo-  
 380     rithm minimizes noise contributions through its seeding process, and including  
 381     the additional layers improves the energy resolution [25]. The cells or clusters are  
 382     associated to a given track if they fall within a cone of  $\Delta R = 0.2$  of the extrapo-  
 383     lated position of the track, which includes about 90% of the energy on average [4].  
 384     This construction is illustrated in Figure 2.

#### 385     8.3.1 E/P DISTRIBUTION

386     The  $E/p$  distributions measured in both data and simulation are shown in Fig-  
 387     ure 3 for two example bins of track momentum and for tracks in the central  
 388     region of the detector. These distributions show several important features of  
 389     the  $E/p$  observable. The large content in the bin at  $E = 0$  comes from tracks that  
 390     have no associated cluster, as mentioned previously these are due to interactions  
 391     with detector material prior to reaching the calorimeter or the energy deposit be-  
 392     ing insufficiently large to generate a seed, and are discussed in Section 8.3.2. The  
 393     small negative tail comes from similar tracks that do not deposit any energy in  
 394     the calorimeter but are randomly associated to a noise cluster. The long positive

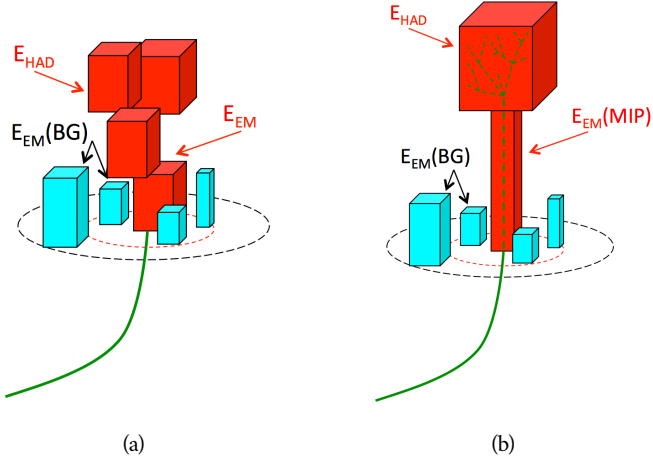


Figure 2: An illustration (a) of the  $E/p$  variable used throughout this paper. The red energy deposits come from the charged particle targeted for measurement, while the blue energy deposits are from nearby neutral particles and must be subtracted. The same diagram (b) for the neutral-background selection, described in Section 8.3.3.

tail above 1.0 comes from the contribution of neutral particles. Nearby neutral particles deposit (sometimes large) additional energy in the calorimeter but do not produce tracks in the inner detector and so they cannot be rejected for isolation. Additionally the peak and mean of the distribution falls below 1.0 because of the loss of energy not found within the cone as well as the non-compensation of the calorimeter.

401 The data and simulation share the same features, but the high and low tails  
402 are significantly different. The simulated events tend to overestimate the contribu-  
403 tion of neutral particle to the long tail, although this effect can be isolated as  
404 discussed in Section 8.3.3. Additionally, the simulated clusters have less noise on  
405 average, although this is a small effect on the overall response.

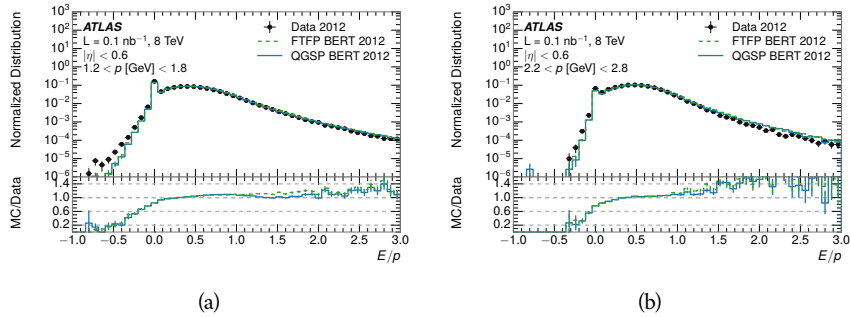


Figure 3: The  $E/p$  distribution and ratio of simulation to data for isolated tracks with (a)  $|\eta| < 0.6$  and  $1.2 < p/\text{GeV} < 1.8$  and (b)  $|\eta| < 0.6$  and  $2.2 < p/\text{GeV} < 2.8$ .

## 406 8.3.2 ZERO FRACTION

407 The fraction of particles with no associated clusters, or similarly those with  $E \leq$   
 408 0, reflects the modelling of both the detector geometry and hadronic interactions.  
 409 The zero fraction is expected to rise as the amount of material a particle traverses  
 410 increases, while it is expected to decrease as the particle energy increases. This  
 411 dependence can be seen in Figure 4, where the zero fraction in data and simula-  
 412 tion is shown as a function of momentum and the amount of material measured  
 413 in interaction lengths. The trends are similar between the 2010 and 2012 mea-  
 414 surements. The zero fraction decreases with energy as expected. The amount of  
 415 material in the detector increases with  $\eta$ , which provides a distribution of in-  
 416 teraction lengths. As the data and simulation have significant disagreement in  
 417 the zero fraction over a number of interaction lengths, the difference must be  
 418 primarily from the modelling of hadronic interactions.

419 There is also a noticeable difference between positive at negative tracks at low  
 420 momentum, which reflects the difference in response between protons and an-  
 421 tiprotons. Antiprotons have significant model differences in the two physics lists,  
 422 QGSP\_BERT and FTFP\_BERT, and this is evident in the lowest momentum bin  
 423 of the data to simulation ratio. This difference is explored further in Section 8.4.

## 424 8.3.3 NEUTRAL BACKGROUND SUBTRACTION

425 The isolation requirement on hadrons is only effective in remove energy contri-  
 426 bution from nearby charged particles. Nearby neutral particles, predominantly  
 427 photons from  $\pi^0$  decays, also add their energy to the calorimeter clusters, but  
 428 mostly in the electromagnetic calorimeter. It is possible to measure this contri-  
 429 bution, on average, using late-showering hadrons that minimally ionize in the  
 430 electromagnetic calorimeter. Such particles are selected by requiring that they  
 431 deposit less than 1.1 GeV in the EM calorimeter within a cone of  $\Delta R < 0.1$   
 432 around the track. To ensure that these particles are well measured, they are addi-  
 433 tionally required to deposit between 40% and 90% of their energy in the hadronic  
 434 calorimeter within the same cone.

435 These particle provide a clean sample to measure the nearby neutral back-  
 436 ground because they do not deposit energy in the area immediately surrounding  
 437 them in the EM calorimeter, as shown in Figure 2. So, the energy deposits in the  
 438 region  $0.1 < \Delta R < 0.2$  can be attributed to neutral particles alone. To estimate  
 439 the contribution to the whole cone considered for the response measurement,  
 440 that energy is scaled by a geometric factor of 4/3. This quantity,  $\langle E/p \rangle_{\text{BG}}$ , mea-  
 441 sured in aggregate over a number of particles, gives the contribution to  $\langle E/p \rangle$   
 442 from neutral particles in the EM calorimeter. Similar techniques were used in  
 443 the individual layers of the hadronic calorimeters to show that the background  
 444 from neutrals is negligible in those layers [4].

445 The distribution of this background estimate is shown in Figure 5. Although  
 446 the simulation captures the overall trend, it significantly overestimates the neu-  
 447 tral contribution for tracks with momentum between 2 and 8 GeV. This effect  
 448 was also seen in the tails of the  $E/p$  distributions in Figure 3. This difference is

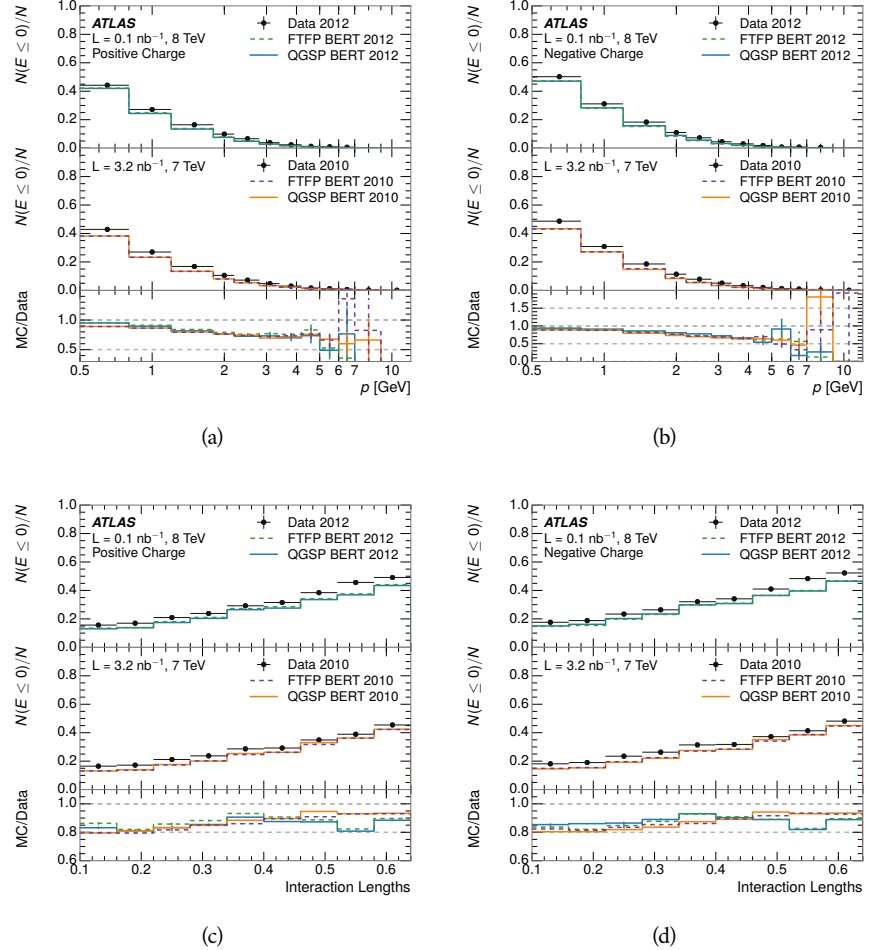


Figure 4: The fraction of tracks as a function (a, b) of momentum, (c, d) of interaction lengths with  $E \leq 0$  for tracks with positive (on the left) and negative (on the right) charge.

likely due to the modelling of coherent neutral particle radiation in Pythia8, as the discrepancy does not depend on  $\eta$  and thus is unlikely to be a mismodelling of the detector. This difference can be subtracted however, to form  $\langle E/p \rangle_{\text{COR}} \equiv \langle E/p \rangle - \langle E/p \rangle_{\text{BG}}$ , which measures the average calorimeter response without the contamination of neutral particles.

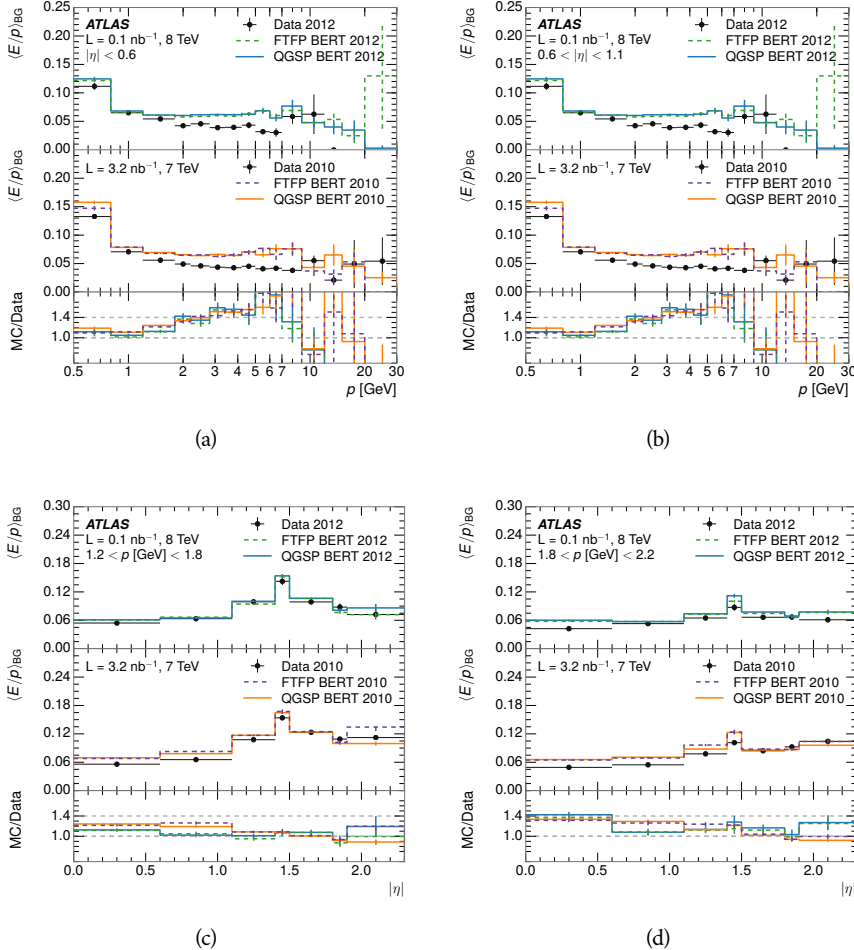


Figure 5:  $\langle E/p \rangle_{\text{BG}}$  as a function of the track momentum and (a)  $|\eta| < 0.6$ , (b)  $0.6 < |\eta| < 1.1$ , and as a function of the track pseudorapidity and (c)  $1.2 < p/\text{GeV} < 1.8$ , (d)  $1.8 < p/\text{GeV} < 2.2$ .

#### 454 8.3.4 CORRECTED RESPONSE

##### 455 8.3.4.1 CLUSTERING

##### 456 8.3.4.2 ADDITIONAL STUDIES

#### 457 8.4 IDENTIFIED PARTICLE RESPONSE



# 9

458

459 JET ENERGY RESPONSE AND UNCERTAINTY

---

460 9.1 JET ENERGY RESPONSE IN SIMULATION

461 9.2 JET ENERGY UNCERTAINTY



462

## PART V

463

### SEARCH FOR LONG-LIVED PARTICLES

464

You can put some informational part preamble text here.



# 10

465

466 LONG-LIVED PARTICLES IN ATLAS

---

467 10.1 OVERVIEW AND CHARACTERISTICS

468 10.2 SIMULATION



469

470 EVENT SELECTION

---

471 11.1 TRIGGER

472 11.2 KINEMATICS AND ISOLATION

473 11.3 STANDARD MODEL REJECTION

474 11.4 IONIZATION

475 11.4.1 DE/DX CALIBRATION

476 11.4.2 MASS ESTIMATION



# 12

477

478 BACKGROUND ESTIMATION

---

479 12.1 BACKGROUND SOURCES

480 12.2 PREDICTION METHOD

481 12.3 VALIDATION AND UNCERTAINTY



# 13

482

483 SYSTEMATIC UNCERTAINTIES AND RESULTS

---

484 13.1 SYSTEMATIC UNCERTAINTIES

485 13.2 FINAL YIELDS



# 14

486

## 487 INTERPRETATION

---

488 14.1 CROSS SECTIONAL LIMITS

489 14.2 MASS LIMITS

490 14.3 CONTEXT FOR LONG-LIVED SEARCHES



491

## PART VI

492

### CONCLUSIONS

493

You can put some informational part preamble text here.



# 15

494

## 495 SUMMARY AND OUTLOOK

---

### 496 15.1 SUMMARY

### 497 15.2 OUTLOOK



498

## PART VII

499

## APPENDIX

500



# A

501

502 INELASTIC CROSS SECTION

---



# B

503

## 504 APPENDIX TEST

---

505 Examples: *Italics*, SMALL CAPS, ALL CAPS <sup>1</sup>. Acronym testing: **UML!** (**UML!**) –  
506 **UML! – UML! (UML!) – UML!s**

This appendix is temporary and is here to be used to check the style of the document.

### 507 B.1 APPENDIX SECTION TEST

508 Random text that should take up a few lines. The purpose is to see how sections  
509 and subsections flow with some actual context. Without some body copy be-  
510 tween each heading it can be difficult to tell if the weight of the fonts, styles,  
511 and sizes use work well together.

#### 512 B.1.1 APPENDIX SUBECTION TEST

513 Random text that should take up a few lines. The purpose is to see how sections  
514 and subsections flow with some actual context. Without some body copy be-  
515 tween each heading it can be difficult to tell if the weight of the fonts, styles,  
516 and sizes use work well together.

### 517 B.2 A TABLE AND LISTING

518 Curabitur tellus magna, porttitor a, commodo a, commodo in, tortor. Donec in-  
519 terdum. Praesent scelerisque. Maecenas posuere sodales odio. Vivamus metus la-  
520 cus, varius quis, imperdiet quis, rhoncus a, turpis. Etiam ligula arcu, elementum a,  
521 venenatis quis, sollicitudin sed, metus. Donec nunc pede, tincidunt in, venenatis  
522 vitae, faucibus vel, nibh. Pellentesque wisi. Nullam malesuada. Morbi ut tellus ut  
523 pede tincidunt porta. Lorem ipsum dolor sit amet, consectetur adipiscing elit.  
524 Etiam congue neque id dolor.

525 There is also a Python listing below Listing 1.

---

1 Footnote example.

LABITUR BONORUM PRI NO	QUE VISTA	HUMAN
fastidii ea ius	germano	demonstratea
suscipit instructior	titulo	personas
quaestio philosophia	facto	demonstrated

Table 1: Autem usu id.

## 526 B.3 SOME FORMULAS

Due to the statistical nature of ionisation energy loss, large fluctuations can occur in the amount of energy deposited by a particle traversing an absorber element<sup>2</sup>. Continuous processes such as multiple scattering and energy loss play a relevant role in the longitudinal and lateral development of electromagnetic and hadronic showers, and in the case of sampling calorimeters the measured resolution can be significantly affected by such fluctuations in their active layers. The description of ionisation fluctuations is characterised by the significance parameter  $\kappa$ , which is proportional to the ratio of mean energy loss to the maximum allowed energy transfer in a single collision with an atomic electron:

*You might get unexpected results using math in chapter or section heads. Consider the pdfspacing option.*

$$\kappa = \frac{\xi}{E_{\max}} \quad (1)$$

$E_{\max}$  is the maximum transferable energy in a single collision with an atomic electron.

$$E_{\max} = \frac{2m_e\beta^2\gamma^2}{1 + 2\gamma m_e/m_x + (m_e/m_x)^2},$$

527 where  $\gamma = E/m_x$ ,  $E$  is energy and  $m_x$  the mass of the incident particle,  $\beta^2 =$   
 528  $1 - 1/\gamma^2$  and  $m_e$  is the electron mass.  $\xi$  comes from the Rutherford scattering  
 529 cross section and is defined as:

$$\xi = \frac{2\pi z^2 e^4 N_{Av} Z \rho \delta x}{m_e \beta^2 c^2 A} = 153.4 \frac{z^2}{\beta^2} \frac{Z}{A} \rho \delta x \text{ keV},$$

530 where

531  $z$  charge of the incident particle  
 532  $N_{Av}$  Avogadro's number  
 533  $Z$  atomic number of the material  
 534  $A$  atomic weight of the material  
 535  $\rho$  density  
 $\delta x$  thickness of the material  
 532  $\kappa$  measures the contribution of the collisions with energy transfer close to  
 533  $E_{\max}$ . For a given absorber,  $\kappa$  tends towards large values if  $\delta x$  is large and/or if  
 534  $\beta$  is small. Likewise,  $\kappa$  tends towards zero if  $\delta x$  is small and/or if  $\beta$  approaches  
 535 1.

2 Examples taken from Walter Schmidt's great gallery:  
<http://home.vrweb.de/~was/mathfonts.html>

Listing 1: A floating example (listings manual)

---

```
1 for i in xrange(10):
    print i, i*i, i*i*i
print "done"
```

---

536      The value of  $\kappa$  distinguishes two regimes which occur in the description of  
537      ionisation fluctuations:

- 538      1. A large number of collisions involving the loss of all or most of the incident  
539      particle energy during the traversal of an absorber.

540      As the total energy transfer is composed of a multitude of small energy  
541      losses, we can apply the central limit theorem and describe the fluctua-  
542      tions by a Gaussian distribution. This case is applicable to non-relativistic  
543      particles and is described by the inequality  $\kappa > 10$  (i. e., when the mean  
544      energy loss in the absorber is greater than the maximum energy transfer  
545      in a single collision).

- 546      2. Particles traversing thin counters and incident electrons under any condi-  
547      tions.

548      The relevant inequalities and distributions are  $0.01 < \kappa < 10$ , Vavilov  
549      distribution, and  $\kappa < 0.01$ , Landau distribution.



550 BIBLIOGRAPHY

---

- 551 [1] ATLAS Collaboration. “The ATLAS Simulation Infrastructure”. In: *Eur.*  
552 *Phys. J. C* 70 (2010), p. 823. doi: [10.1140/epjc/s10052-010-1429-9](https://doi.org/10.1140/epjc/s10052-010-1429-9).  
553 arXiv: [1005.4568 \[hep-ex\]](https://arxiv.org/abs/1005.4568).
- 554 [2] ATLAS Collaboration. “A study of the material in the ATLAS inner de-  
555 tector using secondary hadronic interactions”. In: *JINST* 7 (2012), P01013.  
556 doi: [10.1088/1748-0221/7/01/P01013](https://doi.org/10.1088/1748-0221/7/01/P01013). arXiv: [1110.6191 \[hep-ex\]](https://arxiv.org/abs/1110.6191).
- 557 [3] ATLAS Collaboration. *Summary of ATLAS Pythia 8 tunes*. ATL-PHYS-PUB-  
558 2012-003. 2012. url: <http://cds.cern.ch/record/1474107>.
- 559 [4] ATLAS Collaboration. “Single hadron response measurement and calorime-  
560 ter jet energy scale uncertainty with the ATLAS detector at the LHC”. In:  
561 *Eur. Phys. J. C* 73 (2013), p. 2305. doi: [10.1140/epjc/s10052-013-2305-1](https://doi.org/10.1140/epjc/s10052-013-2305-1). arXiv: [1203.1302 \[hep-ex\]](https://arxiv.org/abs/1203.1302).
- 562 [5] ATLAS Collaboration. “Electron and photon energy calibration with the  
563 ATLAS detector using LHC Run 1 data”. In: *Eur. Phys. J. C* 74 (2014), p. 3071.  
564 doi: [10.1140/epjc/s10052-014-3071-4](https://doi.org/10.1140/epjc/s10052-014-3071-4). arXiv: [1407.5063](https://arxiv.org/abs/1407.5063)  
566 [hep-ex].
- 567 [6] ATLAS Collaboration. “Topological cell clustering in the ATLAS calorime-  
568 ters and its performance in LHC Run 1”. In: (2016). arXiv: [1603.02934](https://arxiv.org/abs/1603.02934)  
569 [hep-ex].
- 570 [7] S. Agostinelli et al. “GEANT4: A simulation toolkit”. In: *Nucl. Instrum. Meth.*  
571 *A* 506 (2003), pp. 250–303. doi: [10.1016/S0168-9002\(03\)01368-8](https://doi.org/10.1016/S0168-9002(03)01368-8).
- 572 [8] N. S. Amelin et al. “Transverse flow and collectivity in ultrarelativistic  
573 heavy-ion collisions”. In: *Phys. Rev. Lett.* 67 (1991), p. 1523. doi: [10.1103/PhysRevLett.67.1523](https://doi.org/10.1103/PhysRevLett.67.1523).
- 574 [9] N. S. Amelin et al. “Collectivity in ultrarelativistic heavy ion collisions”. In:  
575 *Nucl. Phys. A* 544 (1992), p. 463. doi: [10.1016/0375-9474\(92\)90598-E](https://doi.org/10.1016/0375-9474(92)90598-E).
- 576 [10] B. Andersson, A. Tai, and B.-H. Sa. “Final state interactions in the (nuclear)  
577 FRITIOF string interaction scenario”. In: *Z. Phys. C* 70 (1996), pp. 499–  
578 506. doi: [10.1007/s002880050127](https://doi.org/10.1007/s002880050127).
- 579 [11] B. Andersson et al. “A model for low-pT hadronic reactions with general-  
580 izations to hadron-nucleus and nucleus-nucleus collisions”. In: *Nucl. Phys.*  
581 *B* 281 (1987), p. 289. doi: [10.1016/0550-3213\(87\)90257-4](https://doi.org/10.1016/0550-3213(87)90257-4).
- 582 [12] H. W. Bertini and P. Guthrie. “News item results from medium-energy  
583 intranuclear-cascade calculation”. In: *Nucl. Instr. and Meth. A* 169 (1971),  
584 p. 670. doi: [10.1016/0375-9474\(71\)90710-X](https://doi.org/10.1016/0375-9474(71)90710-X).

- 587 [13] L. V. Bravin et al. “Scaling violation of transverse flow in heavy ion colli-  
 588 sions at AGS energies”. In: *Phys. Lett. B* 344 (1995), p. 49. doi: [10.1016/0370-2693\(94\)01560-Y](https://doi.org/10.1016/0370-2693(94)01560-Y).
- 590 [14] L. V. Bravina et al. “Fluid dynamics and Quark Gluon string model - What  
 591 we can expect for Au+Au collisions at 11.6 AGeV/c”. In: *Nucl. Phys. A* 566  
 592 (1994), p. 461. doi: [10.1016/0375-9474\(94\)90669-6](https://doi.org/10.1016/0375-9474(94)90669-6).
- 593 [15] H. S. Fesefeldt. *GHEISHA program*. Pitha-85-02, Aachen. 1985.
- 594 [16] G. Folger and J.P. Wellisch. “String parton models in Geant4”. In: (2003).  
 595 arXiv: [nucl-th/0306007](https://arxiv.org/abs/nucl-th/0306007).
- 596 [17] B. Ganhuyag and V. Uzhinsky. “Modified FRITIOF code: Negative charged  
 597 particle production in high energy nucleus nucleus interactions”. In: *Czech.  
 598 J. Phys.* 47 (1997), pp. 913–918. doi: [10.1023/A:1021296114786](https://doi.org/10.1023/A:1021296114786).
- 599 [18] M. P. Guthrie, R. G. Alsmiller, and H. W. Bertini. “Calculation of the cap-  
 600 ture of negative pions in light elements and comparison with experiments  
 601 pertaining to cancer radiotherapy”. In: *Nucl. Instrum. Meth.* 66 (1968), pp. 29–  
 602 36. doi: [10.1016/0029-554X\(68\)90054-2](https://doi.org/10.1016/0029-554X(68)90054-2).
- 603 [19] V.A. Karmanov. “Light Front Wave Function of Relativistic Composite  
 604 System in Explicitly Solvable Model”. In: *Nucl. Phys. B* 166 (1980), p. 378.  
 605 doi: [10.1016/0550-3213\(80\)90204-7](https://doi.org/10.1016/0550-3213(80)90204-7).
- 606 [20] A.D. Martin, W.J. Stirling, R.S. Thorne, and G. Watt. “Parton distributions  
 607 for the LHC”. In: *Eur. Phys. J. C* 63 (2009). Figures from the **MSTW** Website,  
 608 pp. 189–285. doi: [10.1140/epjc/s10052-009-1072-5](https://doi.org/10.1140/epjc/s10052-009-1072-5). arXiv: [0901.0002](https://arxiv.org/abs/0901.0002).
- 610 [21] B. Nilsson-Almqvist and E. Stenlund. “Interactions Between Hadrons and  
 611 Nuclei: The Lund Monte Carlo, Fritiof Version 1.6”. In: *Comput. Phys. Com-  
 612 mun.* 43 (1987), p. 387. doi: [10.1016/0010-4655\(87\)90056-7](https://doi.org/10.1016/0010-4655(87)90056-7).
- 613 [22] A. Ribon et al. *Status of Geant4 hadronic physics for the simulation of LHC  
 614 experiments at the start of LHC physics program*. CERN-LCGAPP-2010-02.  
 615 2010. URL: <http://lcgapp.cern.ch/project/docs/noteStatusHadronic2010.pdf>.
- 617 [23] A. Sherstnev and R.S. Thorne. “Parton Distributions for LO Generators”.  
 618 In: *Eur. Phys. J. C* 55 (2008), pp. 553–575. doi: [10.1140/epjc/s10052-008-0610-x](https://doi.org/10.1140/epjc/s10052-008-0610-x). arXiv: [0711.2473](https://arxiv.org/abs/0711.2473).
- 620 [24] T. Sjöstrand, S. Mrenna, and P. Skands. “A Brief Introduction to PYTHIA  
 621 8.1”. In: *Comput. Phys. Commun.* 178 (2008), pp. 852–867. doi: [10.1016/j.cpc.2008.01.036](https://doi.org/10.1016/j.cpc.2008.01.036). arXiv: [0710.3820](https://arxiv.org/abs/0710.3820).
- 623 [25] Peter Speckmayer. “Energy Measurement of Hadrons with the CERN AT-  
 624 LAS Calorimeter”. Presented on 18 Jun 2008. PhD thesis. Vienna: Vienna,  
 625 Tech. U., 2008. URL: <http://cds.cern.ch/record/1112036>.

626 DECLARATION

---

627 Put your declaration here.

628 *Berkeley, CA, September 2016*

629

---

Bradley Axen



<sup>631</sup> COLOPHON

Not sure that this is necessary.